$X/H = 1$. Because of space limitations, only predicted results by LRR, IPCM, and SSG on the free vortex case are presented here. By examining the distributions of $\overline{uv}$, one can observe that a higher level of shear stress was predicted by the IPCM model compared with LRR and SSG. This phenomenon is consistent with the previously observed centerline axial velocity development, indicating IPCM has a faster rate of flow recovery. The cause of this behavior can be traced back to the formulation of the modeled form of the pressure-strain process. The pressure-strain term of $\overline{uv}$ of the SSG model can be expressed in terms of that of IPCM and is as

$$(\phi_{\overline{uv}})_{\mathrm{SSG}} = (\phi_{\overline{uv}})_{\mathrm{IPCM}} + \underbrace{\epsilon\left(0.2 - 1.8\frac{P_k}{\epsilon}\right)b_{12}}_{A} + \underbrace{4.2\epsilon[(b_{11}+b_{22})b_{12}+b_{13}b_{23}]}_{B} - \underbrace{0.65\sqrt{b_{kl}b_{kl}}k\frac{\partial U}{\partial R}}_{C} + \underbrace{k(0.425b_{11}-0.375b_{22})\frac{\partial U}{\partial R}}_{D} + \underbrace{kb_{13}\left(0.425\frac{\partial W}{\partial R}+1.575\frac{W}{R}\right)}_{E} \tag{1}$$

where $b_{ij} = \overline{u_i u_j}/\overline{u_k u_k} - 1/3\delta_{ij}$ and the wall reflection terms of IPCM have been neglected. Terms B and C and the production related part of term A do not exist in the linear pressure-strain models.

Attention is now directed to the shear layer at $R/H = 0.8$ of the free vortex case, shown in Fig. 2. It is clear that the major terms A, D, and E act as extra sink terms, relative to the IPCM model, for the modeled $\overline{uv}$ equation adopting the SSG model. Across the nonequilibrium shear layer where the production term P_k is much higher than the turbulence dissipation rate ϵ, this makes the effect of term A even more pronounced. At $R/H = 2.2$, the lower level of $\overline{uv}$ predicted by the SSG model is consistent with what was observed at $R/H = 0.8$, albeit the SSG result is now closer to measurements. This conforms to preliminary computations of nonswirling sudden-expanding pipe flow, in which case SSG results were not only lower than the IPCM results but also closer to measurements. The lack of wall reflection terms in the SSG did not contribute to the predicted depressed level of $\overline{uv}$, for the terms, if present, would further reduce the level of shear stress near the wall. Comparing the level of predicted $\overline{uv}$ by the SSG model at $R/H = 0.8$ and 2.2, one can observe that at $R/H = 0.8$, the predicted level of shear stress is excessively depressed. This may be attributed to the fact that the influence of term E, which is related to swirl and $\overline{uw}$, is active only at $R/H = 0.8$. A better level of $\overline{uw}$ is also predicted by the IPCM model, and this can also be attributed to the pressure-strain modeling. The LRR model predicted the wrong sign of the stress $\overline{uw}$ around the region $R/H = 2.2$, where IPCM returned the best results.

Conclusion

Computations of turbulent swirling flows inside a dump combustor model were performed by the k-ϵ model and variants of the Reynolds stress transport model with linear (IPGY, IPGL, and IPCM) and quadratic (SSG) forms of the pressure-strain models. Comparisons of predictions with measurements indicated that IPCM performed best, in terms of mean and turbulence results. The slower axial flow recovery predicted by SSG and LRR was attributed to the lower level of $\overline{uv}$ predicted by the models, and this could be traced back to the modeled form of the pressure-strain term, after examining the formulations of the pressure-strain models.

Acknowledgments

This research work was supported by the National Science Council of Taiwan under Grant NSC-82-0401-E-007-251. The computational facilities were provided by the National Centre for High-Performance Computing of Taiwan, which the authors gratefully acknowledge.

References

[1]Gibson, M. M., and Younis, B. A., "Calculation of Swirling Jet with a Reynolds Stress Closure," *Physics of Fluids*, Vol. 29, No. 1, 1986, pp. 38–48.

[2]Fu, S., Launder, B. E., and Leschziner, M. A., "Modelling Strongly Swirling Recirculating Jet with Reynolds-Stress Transport Closure," *Proceedings of the 6th Symposium on Turbulent Shear Flows* (Toulouse, France), Université Paul Sabatier, Toulouse, France, 1987, pp. 17.6.1–17.6.6.

[3]Younis, B. A., Gatski, T. B., and Speziale, C. G., "On the Prediction of Free Turbulent Jets with Swirl Using a Quadratic Pressure-Strain Model," Inst. for Computer Applications in Science and Engineering, Rept. 94-70. Hampton, VA, Aug. 1994.

[4]Lin, C. A., and Leschziner, M. A., "Three-Dimensional Computation of Transient Interaction Between Radially Injected Jet and Swirling Cross-Flow Using Second-Moment Closure," *Computational Fluid Dynamics Journal*, Vol. 1, No. 4, 1993, pp. 423–432.

[5]Gibson, M. M., and Launder, B. E., "Ground Effects on Pressure Fluctuations in the Atmospheric Boundary Layer," *Journal of Fluid Mechanics*, Vol. 86, June 1978, pp. 491–511.

[6]Launder, B. E., Reece, G. J., and Rodi, W., "Progress in the Development of a Reynolds-Stress Turbulence Closure," *Journal of Fluid Mechanics*, Vol. 68, June 1975, pp. 537–566.

[7]Speziale, C. G., Sarkar, S., and Gatski, T. B., "Modelling the Pressure-Strain Correlation of Turbulence: An Invariant Dynamical Approach," *Journal of Fluid Mechanics*, Vol. 227, June 1991, pp. 245–272.

[8]Patankar, S. V., and Spalding, D. B., "A Calculation Procedure for Heat, Mass and Momentum Transfer in Three-Dimensional Parabolic Flows," *International Journal of Heat and Mass Transfer*, Vol. 15, Oct. 1972, pp. 1787–1806.

[9]Leonard, B. P., "A Stable and Accurate Convective Modelling Procedure Based on Quadratic Upstream Interpolation," *Computer Methods in Applied Mechanics and Engineering*, Vol. 19, June 1979, pp. 59–98.

[10]Ahmed, S. A., and Nejad, A. S., "Swirl Effects on Confined Flows in Axisymmetric Geometries," *Journal of Propulsion and Power*, Vol. 8, No. 2, 1992, pp. 339–345.

Prediction of Aerodynamic Flows with a New Explicit Algebraic Stress Model

Ridha Abid*
High Technology Corporation, Hampton, Virginia 23666
Joseph H. Morrison*
Analytical Services and Materials, Inc., Hampton, Virginia 23666
Thomas B. Gatski*
NASA Langley Research Center, Hampton, Virginia 23681-0001
and
Charles G. Speziale†
Boston University, Boston, Massachusetts 02215

I. Introduction

COMPUTATIONAL fluid dynamics (CFD) has become an increasingly powerful tool in the aerodynamic design of aerospace vehicles as a result of improvements in numerical algorithms and computer capacity. Major future gains in efficiency are expected to come about as massively parallel supercomputer technology matures. However, some critical pacing items limit the effectiveness of CFD in engineering applications. Chief among these items is turbulence modeling. Numerous turbulence models of varying degrees of complexity, which can be classified as ranging from eddy-viscosity models to full Reynolds stress closures, have been proposed (see Refs. 1 and 2 for reviews).

Received Feb. 26, 1996; revision received June 16, 1996; accepted for publication Aug. 21, 1996; also published in *AIAA Journal on Disc*, Volume 2, Number 1. This paper is declared a work of the U.S. Government and is not subject to copyright protection in the United States.

*Senior Scientist. Member AIAA.
†Professor of Aerospace and Mechanical Engineering. Member AIAA.

Debates continue to rage over which turbulence models are the best while it is clear that they all have at least some deficiencies. Two-equation models have represented a good compromise between the simplicity of empirical mixing length models and the complexity of full Reynolds stress (i.e., second-order) closures. This explains the popularity of the standard K–ε model of Launder and Spalding.[3] Because modeled transport equations are solved for the turbulent kinetic energy and dissipation rate, at least some history and nonlocal effects are incorporated. However, the standard K–ε model still uses an eddy-viscosity representation for the Reynolds stresses that omits a lot of turbulence physics. Anisotropic eddy-viscosity models have been proposed during the past decade to overcome this deficiency while maintaining the two-equation format of the K–ε model.[4,5] Most notable among these are the explicit algebraic stress models (EASMs) that are formally obtained from full second-order closures in the homogeneous, equilibrium limit. First obtained by Pope[6]—and later generalized by Gatski and Speziale[7]—EASMs are obtained via an integrity bases solution of a generalization of the implicit algebraic stress model (ASM) of Rodi.[8] Because they formally constitute two-equation models with an anisotropic eddy viscosity (and strain-dependent coefficients), they maintain the relative simplicity of the K–ε model while incorporating more turbulence physics. For turbulent flows that are close to equilibrium, these EASMs yield results that are almost indistinguishable from those obtained with a full second-order closure.[7]

In a recent paper, Abid et al.[9] reported calculations of separated airfoil flows based on an EASM. However, in that preliminary study, the pressure-strain model of Launder et al.[10] was used because of its widespread popularity. The purpose of the present note is to present an EASM based on the more current pressure-strain model of Speziale et al.[11] (the SSG model). The SSG model represents a recent upgrade of the Launder et al.[10] model that does not require wall reflection terms. The ability of the proposed model to predict nonequilibrium flows over an airfoil and a wing will be established. The ISAAC Navier–Stokes code[12] is used to simulate the flows considered.

II. Theoretical Analysis

For a weakly compressible turbulence at high Reynolds numbers, the Reynolds stress tensor $\tau_{ij} = \overline{u_i u_j}$ is a solution of the transport equation[13]

$$\bar{\rho}\frac{\mathrm{D}\tau_{ij}}{\mathrm{D}t} = -\bar{\rho}\left(\tau_{ik}\frac{\partial \bar{u}_j}{\partial x_k} + \tau_{jk}\frac{\partial \bar{u}_i}{\partial x_k}\right) + \Pi_{ij} - \frac{2}{3}\bar{\rho}\varepsilon\delta_{ij} + D_{ij}^T + \mu\nabla^2\tau_{ij} \tag{1}$$

where Π_{ij} is the deviatoric part of the pressure-strain correlation, D_{ij}^T is the turbulent transport term, ε is the turbulent dissipation rate, μ is the viscosity, $\bar{u}_i$ is the mean-velocity component, and $\bar{\rho}$ is the mean density. Explicit compressibility effects are neglected in Eq. (1). Evidence has indicated that this assumption can be applied if the external Mach number M_∞ is not extremely large (usually, $M_\infty < 5$).

If we contract the indices in Eq. (1), then we obtain the transport equation for the turbulent kinetic energy, $K = \frac{1}{2}\overline{u_i u_i}$:

$$\bar{\rho}\frac{\mathrm{D}K}{\mathrm{D}t} = \bar{\rho}P - \bar{\rho}\varepsilon + D_K^T + \mu\nabla^2 K \tag{2}$$

where $P = -\tau_{ij}\partial\bar{u}_i/\partial x_j$ is the turbulence production term, ε is the turbulent dissipation rate, and D_K^T is the turbulent transport term obtained from a contraction of D_{ij}^T.

Rodi,[8] following the paper of Launder and Ying,[14] proposed the idea of the ASM, which provides algebraic equations in lieu of solving differential equations for the Reynolds stresses. He effectively assumed that

$$\frac{\mathrm{D}b_{ij}}{\mathrm{D}t} = 0, \qquad {}_D\left(D_{ij}^T + v\nabla^2\tau_{ij}\right) = 0 \tag{3}$$

where

$$b_{ij} = \frac{\tau_{ij} - \frac{2}{3}K\delta_{ij}}{2K} \tag{4}$$

is the Reynolds stress anisotropy and ${}_D(\cdot)$ represents the deviatoric part. Thus, turbulent diffusion is neglected in the evolution of the Reynolds stress anisotropies, which are assumed to be in equilibrium.

The substitution of Eq. (3) into Eq. (1) yields the following algebraic stress equation:

$$(P-\varepsilon)b_{ij} = -\tfrac{2}{3}K\left(S_{ij} - \tfrac{1}{3}S_{kk}\delta_{ij}\right) - K\left(b_{ik}S_{jk} + b_{jk}S_{ik} - \tfrac{2}{3}b_{mn}S_{mn}\delta_{ij}\right) - K(b_{ik}W_{jk} + b_{jk}W_{ik}) + (\Pi_{ij}/2\bar{\rho}) \tag{5}$$

where

$$S_{ij} = \frac{1}{2}\left(\frac{\partial\bar{u}_i}{\partial x_j} + \frac{\partial\bar{u}_j}{\partial x_i}\right), \qquad W_{ij} = \frac{1}{2}\left(\frac{\partial\bar{u}_i}{\partial x_j} - \frac{\partial\bar{u}_j}{\partial x_i}\right) \tag{6}$$

are, respectively, the mean-rate-of-strain tensor and mean-vorticity tensor. Given a pressure-strain-correlation model, Eq. (5) provides an implicit algebraic equation for the determination of the Reynolds stress tensor τ_{ij}. Computations that use this implicit model indicated that stable numerical solutions can be difficult to obtain at times. Hence, an EASM that is a mathematically consistent solution to Eq. (5) is preferable.

Pope[6] developed a methodology for obtaining the explicit solution to Eq. (5) by using a tensorial polynomial expansion in the integrity bases. Gatski and Speziale[7] used this method to derive an explicit algebraic stress equation for two- and three-dimensional turbulent flows. To generalize their results, they applied their algebraic stress representation to the general class of pressure-strain correlation models for Π_{ij} that are linear in the anisotropy tensor b_{ij}. The general linear form of Π_{ij} is

$$\Pi_{ij}/\bar{\rho} = -C_1\varepsilon b_{ij} + C_2K\left(S_{ij} - \tfrac{1}{3}S_{kk}\delta_{ij}\right) + C_3K\left(b_{ik}S_{jk} + b_{jk}S_{ik} - \tfrac{2}{3}b_{mn}S_{mn}\delta_{ij}\right) + C_4K(b_{ik}W_{jk} + b_{jk}W_{ik}) \tag{7}$$

The explicit nonlinear constitutive equation, derived by Gatski and Speziale,[7] then is given after regularization by

$$\bar{\rho}\tau_{ij} = \tfrac{2}{3}\bar{\rho}K\delta_{ij} - 2\mu_t^*\left[\left(S_{ij} - \tfrac{1}{3}S_{kk}\delta_{ij}\right) + \alpha_4(K/\varepsilon) \times (S_{ik}W_{kj} + S_{jk}W_{ki}) - \alpha_5(K/\varepsilon)\left(S_{ik}S_{kj} - \tfrac{1}{3}S_{kl}S_{kl}\delta_{ij}\right)\right] \tag{8}$$

where

$$\mu_t^* = \bar{\rho}C_\mu^*(K^2/\varepsilon) \tag{9}$$

$$C_\mu^* = \frac{3(1+\eta^2)\alpha_1}{3+\eta^2+6\eta^2\xi^2+6\xi^2} \tag{10}$$

$$\eta^2 = \alpha_2(S_{ij}S_{ij})(K^2/\varepsilon^2), \qquad \xi^2 = \alpha_3(W_{ij}W_{ij})(K^2/\varepsilon^2) \tag{11}$$

and $\bar{\rho}$ is the mean density. The constants in Eqs. (9–11) are given by

$$\alpha_1 = \left(\tfrac{4}{3} - C_2\right)(g/2), \qquad \alpha_2 = (2-C_3)^2(g^2/4), \qquad \alpha_3 = (2-C_4)^2(g^2/4) \tag{12}$$

$$\alpha_4 = \left(\frac{2-C_4}{2}\right)g, \qquad \alpha_5 = (2-C_3)g, \qquad g = \frac{1}{(C_1/2)+C_5-1} \tag{13}$$

To avoid numerical problems in the initial stages of the computation or in the freestream region, an alternative regularized form of C_μ^* is used herein:

$$C_\mu^* = \alpha_1\frac{3(1+\eta^2)+0.2(\eta^6+\xi^6)}{3+\eta^2+6\eta^2\xi^2+6\xi^2+\eta^6+\xi^6} \tag{14}$$

which is equivalent to Eq. (10) to order η^6 and ξ^6. The relation (14) does not discernibly change the value of C_μ^* under near-equilibrium conditions, but limits C_μ^* to a small nonzero value ($0.2\alpha_1$) for high values of η or ξ to avoid numerical instabilities. In the present study,

the pressure-strain-correlation model of Speziale et al.[11] is considered; the coefficients are

$$C_1 = 6.8, \qquad C_2 = 0.36, \qquad C_3 = 1.25$$
$$C_4 = 0.40, \qquad C_5 = 1.88 \tag{15}$$

The nonlinear constitutive equation (8) must be solved in conjunction with the following modeled transport equations for the turbulent kinetic energy and dissipation rate:

$$\bar{\rho}\frac{\mathrm{D}K}{\mathrm{D}t} = \bar{\rho}P - \bar{\rho}\varepsilon + \frac{\partial}{\partial x_j}\left[\left(\mu + \frac{\mu_t}{\sigma_k}\right)\frac{\partial K}{\partial x_j}\right] \tag{16}$$

$$\bar{\rho}\frac{\mathrm{D}\varepsilon}{\mathrm{D}t} = C_{\varepsilon_1}\bar{\rho}\frac{\varepsilon}{K}P - C_{\varepsilon_2}\bar{\rho}f_2\frac{\varepsilon^2}{K} + \frac{\partial}{\partial x_j}\left[\left(\mu + \frac{\mu_t}{\sigma_\varepsilon}\right)\frac{\partial \varepsilon}{\partial x_j}\right] \tag{17}$$

given that, here, $\mu_t = C^*_{\mu l}\bar{\rho}(K^2/\varepsilon)$ and $C^*_{\mu l}$ (= 0.081) is the equilibrium value of C^*_μ in the logarithmic layer. The coefficients of the model are

$$\sigma_k = 1.0, \qquad \kappa = 0.41, \qquad C_{\varepsilon_1} = 1.44$$
$$C_{\varepsilon_2} = 1.83, \qquad \sigma_\varepsilon = \frac{\kappa^2}{(C_{\varepsilon_2} - C_{\varepsilon_1})\sqrt{C^*_{\mu l}}} \tag{18}$$

and

$$f_2 = \{1 - \exp[-(y^+/5.5)]\}^2, \qquad y^+ = (\rho y u_\tau/\mu) \tag{19}$$

given that u_τ is the shear velocity, y is normal distance to the wall, and μ is the viscosity. Note that the new model can be integrated directly to the wall without adding a damping function to the eddy viscosity. The function f_2 is introduced to simply remove the singularity in the dissipation rate equation at the wall.

At the wall, the boundary conditions for K and ε are given by

$$K = 0, \qquad \varepsilon = 2\nu\left(\frac{\partial\sqrt{K}}{\partial y}\right)^2 \tag{20}$$

III. Results and Discussion

The calculations to be presented were conducted with the three-dimensional ISAAC Navier–Stokes code,[12] which uses a second-order-accurate finite volume scheme. The convective terms are discretized with an upwind scheme that is based on Roe's flux-difference splitting method. All viscous terms are centrally differenced. The equations are integrated in time with an implicit, spatially split approximate-factorization scheme.

The performance of the EASM presented in Sec. II was first tested for the flat-plate turbulent boundary layer at zero-pressure gradient. As expected (for brevity, the results are not shown here), the new model yielded good predictions for the mean-velocity profiles and skin-friction coefficients. Although some turbulence properties near the wall are not accurately captured (e.g., the peak in the turbulent kinetic energy), the new model does give accurate results away from the buffer layer (i.e., for $y^+ > 30$). Remember that the new EASM can be integrated directly to a solid boundary with no wall damping function in the turbulent eddy viscosity.

The first test case to be considered is the RAE 2822 airfoil flow (case 9), which was tested by Cooke et al.[15] The airfoil has a maximum thickness of 12.1% c and a leading-edge radius of 0.827% c (c is the chord length of the airfoil). The grid used is a 257 × 97C mesh with 177 points on the airfoil, and a minimum spacing at the wall of $0.932 \times 10^{-6}c$. The outer boundary extent is approximately 18c, and transition is assumed at 3% c. For case 9, the conditions include a Mach number $M_\infty = 0.73$, an angle of attack $\alpha = 2.8$ deg, and a Reynolds number $Re = 6.5 \times 10^6$. This test case contains no separated flow.

Figures 1 and 2 compare the surface pressure and skin-friction coefficients computed along the airfoil surface with the experimental data for case 9. It is clear that the EASM provides a good representation of the pressure over most of the airfoil. However, the turbulence model overpredicts the skin-friction coefficient downstream of the shock. This deficiency results from the tendency of models based on the K–ε type of formulation to predict excessive near-wall levels of the turbulent length scale in the presence of an adverse pressure gradient, which leads to high values of the eddy viscosity. A

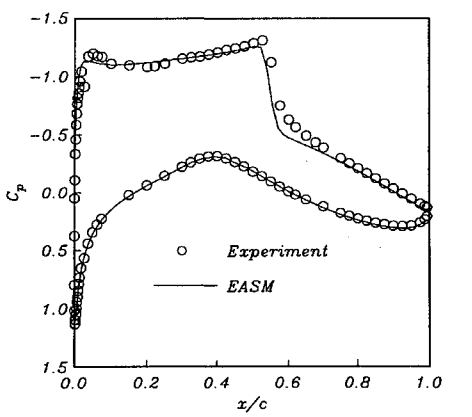

Fig. 1 Surface pressure distributions for RAE 2822 airfoil (case 9).

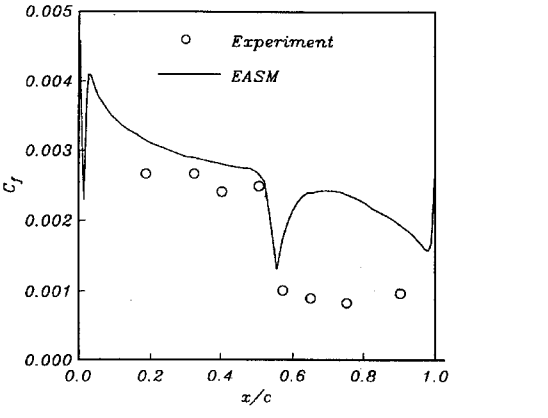

Fig. 2 Skin friction distributions for RAE 2822 airfoil (case 9).

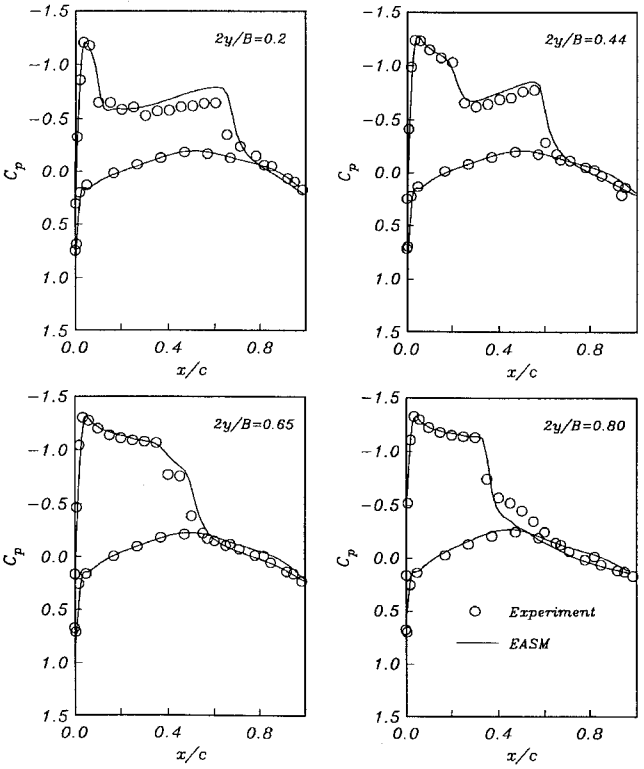

Fig. 3 Surface pressure distributions for ONERA M6 wing.

modification of the dissipation rate equation is required to improve the response of the ASM to adverse pressure-gradient effects.

The second test case to be considered is the ONERA M6 wing at a Mach number $M_\infty = 0.8447$, an angle of attack $\alpha = 5.06$ deg, and a Reynolds number $Re = 11.7 \times 10^6$ based on the mean aerodynamic chord length.[16] A C–O grid used in this study has $193 \times 49 \times 33$ points in the streamwise, normal, and spanwise directions. The minimum normal spacing over the wing of $0.000015\, c_{\text{root}}$ is used and a distance from the wing to the outer boundary of at least $7.95\, c_{\text{root}}$ is considered. No wind-tunnel test corrections are employed for this case. Figure 3 shows a comparison of the computed surface pressure distributions with the experimental data at four different spanwise locations, $2y/B$. It is clear that the shock location and the surface pressure distributions predicted by the EASM are in good agreement with the experimental data and similar to the results reported[17] for the Johnson–King model, which has been highly tuned for airfoil flows. This is an encouraging result.

IV. Conclusion

A new EASM, which is derived from one of the most current second-order closures, has been applied to two aerodynamic test cases—one of which involves separation. The results clearly demonstrate the potential of the new model. Such EASMs have shown some improvement over the standard two-equation models because of their ability to accurately account for mild nonequilibrium effects and to give a realistic representation of the anisotropy of turbulence. However, this improvement still is limited by the dissipation rate equation, which fails to respond properly to adverse pressure gradients. A major research effort to correct this deficiency is currently underway.

Acknowledgments

The first and second authors would like to thank NASA Langley Research Center for support under Contracts NAS1-20059 and NAS1-19831. The fourth author acknowledges the support of the Office of Naval Research under Grant N00014-94-1-0088 (L. P. Purtell, Program Officer).

References

[1]Speziale, C. G., "Analytical Methods for the Development of Reynolds Stress Closures in Turbulence," *Annual Review of Fluid Mechanics*, Vol. 23, 1991, pp. 107–157.

[2]Wilcox, D. C., *Turbulence Modeling for CFD*, DCW Industries, Inc., La Cañada, CA, 1993.

[3]Launder, B. E., and Spalding, D. B., "The Numerical Computation of Turbulent Flows," *Computer Methods in Applied Mechanics and Engineering*, Vol. 3, 1974, pp. 269–289.

[4]Speziale, C. G., "On Nonlinear K–l and K–ε Models of Turbulence," *Journal of Fluid Mechanics*, Vol. 178, 1987, pp. 459–475.

[5]Rubinstein, R., and Barton, J. M., "Nonlinear Reynolds Stress Models and the Renormalization Group," *Physics of Fluids*, Vol. A2, No. 8, 1990, pp. 1472–1476.

[6]Pope, S. B., "A More General Effective Viscosity Hypothesis," *Journal of Fluid Mechanics*, Vol. 72, 1975, pp. 331–340.

[7]Gatski, T. B., and Speziale, C. G., "On Explicit Algebraic Stress Models for Complex Turbulent Flows," *Journal of Fluid Mechanics*, Vol. 254, 1993, pp. 59–78.

[8]Rodi, W., "A New Algebraic Relation for Calculating the Reynolds Stresses," *Zeitschrift für Angewandte Mathematik und Mechanik*, Vol. 56, 1976, pp. T219–T221.

[9]Abid, R., Rumsey, C., and Gatski, T. B., "Prediction of Non-Equilibrium Turbulent Flows with Explicit Algebraic Stress Models," *AIAA Journal*, Vol. 33, No. 11, 1995, pp. 2026–2031.

[10]Launder, B. E., Reece, G. J., and Rodi, W., "Progress in the Development of a Reynolds Stress Turbulence Closure," *Journal of Fluid Mechanics*, Vol. 68, 1975, pp. 537–566.

[11]Speziale, C. G., Sarkar, S., and Gatski, T. B., "Modeling the Pressure-Strain Correlation of Turbulence: An Invariant Dynamical Systems Approach," *Journal of Fluid Mechanics*, Vol. 227, 1991, pp. 245–272.

[12]Morrison, J. H., "A Compressible Navier–Stokes Solver with Two-Equation and Reynolds Stress Turbulence Closure Models," NASA CR4440, May 1992.

[13]Hinze, J. O., *Turbulence*, McGraw–Hill, New York, 1975.

[14]Launder, B., and Ying, Y., "Prediction of Flow and Heat Transfer in Ducts of Square Cross Section," *Proceedings of Institute of Mechanical Engineers*, Vol. 187, 1973, pp. 455–461.

[15]Cooke, P., McDonald, M., and Firmin, M., "Airfoil RAE2822—Pressure Distributions and Boundary Layer Wake Measurements," AGARD AR-138, May 1979.

[16]Schmitt, V., and Charpin, F., "Pressure Distribution on the ONERA M6 Wing at Transonic Mach Numbers," AGARD-AR-138, May 1979.

[17]Rumsey, C., and Vatsa, V. N., "Comparison of the Predictive Capabilities of Several Turbulence Models," *Journal of Aircraft*, Vol. 32, No. 3, 1995, pp. 510–514.

Development of a Rayleigh Scattering Measurement System for Hypersonic Wind-Tunnel Applications

Charles Tyler*
U.S. Air Force Wright Laboratory,
Wright–Patterson Air Force Base, Ohio 45433-7005

Introduction

RAYLEIGH scattering is a nonintrusive measurement technique, which has been used successfully over the last several years for simple reacting flows,[1] combustors,[2] and subsonic freejets.[3] Recently the Rayleigh scattering technique has been extended into the supersonic regime with limited quantitative results. Condensation and cluster formation have been found to have an adverse effect on Rayleigh scatter measurements.[4] Various efforts in eliminating such adverse effects and other unwanted biases, e.g., extraneous scattering off tunnel surfaces, have been made.

Although the construction of baffles for the elimination of stray laser beams has been found by others to reduce background scatter, such constructs do not eliminate laser glare off a model surface completely. Recently, a dual-line Rayleigh scatter system, using the green and yellow lines of a copper-vapor laser, has been developed and tested by Otugen et al.[5] This particular technique identifies and eliminates surface scatter background noise. Other recent techniques, which measure velocity, temperature, and density in supersonic and other high-speed flows, include filtered Rayleigh scattering and Raman excitation and lased-induced fluorescence imaging.[7] Filtered Rayleigh scattering is an alternate way of eliminating background scattering. These techniques solve the problem of surface scatter background noise; however, they do not address the problems associated with flow condensation.

In the past, a substantial amount of research regarding condensation in supercooled hypersonic flow has been performed.[8,9] Recently, Shirinzadeh et al.[10] performed experiments in a 15-in. Mach 6 high-temperature facility with the results that, in the absence of condensation, it is possible to obtain quantitative measurements of density using Rayleigh scattering techniques.

Experiments performed in a Mach 6 high Reynolds number facility were at a lower stagnation temperature of 556 K and higher stagnation pressures of 2.01 and 4.83 MPa. Density profiles, for a select location on a 8-deg half-angle blunt nose cone, obtained by Rayleigh scatter measurements were compared to computational fluid dynamics (CFD) results.

Equipment/Facility Discussion

The Rayleigh scatter measurement system was located at the Mach 6 high Reynolds number facility; an equipment schematic is shown in Fig. 1. A frequency-doubled Nd:YAG pulsed laser pumps two oscillator-amplifier, tunable dye lasers. The output from one

Received April 13, 1996; revision received July 11, 1996; accepted for publication Aug. 29, 1996; also published in *AIAA Journal on Disc*, Volume 2, Number 1. This paper is declared a work of the U.S. Government and is not subject to copyright protection in the United States.

*Aerospace Engineer, Wright Laboratory/Flight Dynamics Directorate/Aeromechanics Division. Member AIAA.